

# DEVELOPMENT OF A FLUORESCENCE BASED GAS SHEET PROFILE MONITOR FOR USE WITH ELECTRON LENSES: OPTICAL SYSTEM DESIGN AND PREPARATORY EXPERIMENTS

S. Udrea<sup>†</sup>, P. Forck, GSI Helmholtzzentrum für Schwerionenforschung, Darmstadt, Germany  
E. Barrios Diaz, N. Chritin, O. R. Jones, P. Magagnin, G. Schneider, R. Veness,  
CERN, Geneva, Switzerland  
V. Tzoganis, C. Welsch, H. Zhang, Cockcroft Institute, Warrington, United Kingdom

## Abstract

A hollow electron lens is presently under study as a possible addition to the collimation system for the high luminosity upgrade of the LHC, while an electron lens system is also proposed for space charge compensation in the SIS-18 synchrotron for the high intensities at the future FAIR facility. For effective operation, a precise alignment is necessary between the high energy hadron beam and the low energy electron beam. In order to achieve this a beam diagnostics set-up based on an intersecting gas sheet and the observation of beam-induced fluorescence is under development. In this contribution we give an account of the design and performance of the optical detection system and report on recent preparatory experiments performed using a laboratory gas curtain set-up.

## BEAM-INDUCED FLUORESCENCE SET-UP OVERVIEW

The beam-induced fluorescence (BIF) set-up for transverse beam diagnostics for electron lenses has as main components a supersonic gas sheet generator and an intensified camera system with an appropriate lens. The supersonic gas sheet is supposed to cross the charged particle beams under consideration and emit fluorescence radiation as a consequence of the interaction between the charged particles and the gas atoms or molecules. Part of the emitted radiation is collected by the lens and an image of the interaction region and thus of the transversal beam profiles is formed at the detector of the camera system.

The electron lens under study for the future high luminosity upgrade of the LHC (HL-LHC) will generate a hollow, 5 A, 10 keV electron beam which will be stabilized around the axis of the high energy proton beam by a 4 T magnetic field produced by a superconducting solenoid. Presently two BIF stations are foreseen, one at each end of the solenoid. At these positions the electron beam will not be in full compression, so is expected to have an outer diameter of approximately 10.5 mm and an inner one of about 7 mm, while the proton beam will have a sigma of approximately 0.3 mm. Thus the gas sheet is planned to have a width of about 11 mm and a thickness of less than 1 mm to allow for a proper interaction region. As working gases both Nitrogen [1] and Neon are

presently under consideration. A 3D model of the diagnostics test set-up using a low current electron beam is shown in Fig. 1. This prototype is planned for commissioning at the Cockcroft Institute, UK towards the end of 2017.

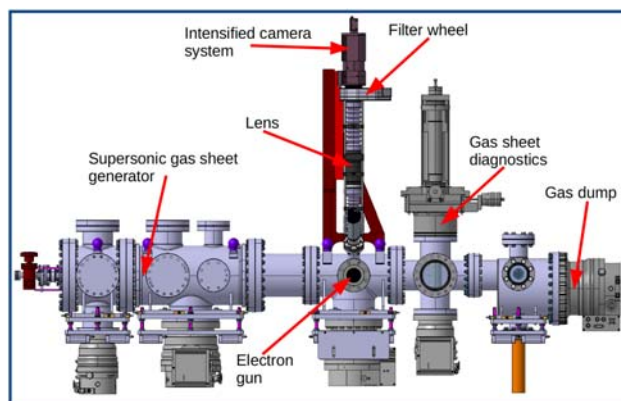


Figure 1: 3D model of the full prototype set-up to be commissioned end of 2017. An electron beam generated by a commercially available electron gun will be used for testing purposes.

## THE INTENSIFIED CAMERA SYSTEM

The cross-sections and integration times estimated for both Nitrogen [1] and Neon show that a camera system with the capability to detect single photons is required. Recent studies carried out at GSI [2] showed that an image intensifier based on MCP technology is currently still the best choice. Thus a ProxiKit PKS 2581 TZ-V image intensifier made by ProxiVision and using a  $\varnothing 1''$  double MCP in Chevron configuration has been acquired. Its main characteristics are:

- UV enhanced S20 photocathode, see Fig. 2 for sensitivity dependence upon wavelength
- P43 phosphor screen
- 28 lp/mm (line pairs per mm) maximum spatial resolution at the phosphor screen plane
- gated, TTL-triggered HV supply, minimum gate time 25  $\mu$ s, no limit is imposed to the maximum, repetition rate up to 1 kHz
- Schneider Componon 12 35/2.8 lens system as optical relay to image the phosphor screen on a camera sensor
- C-mount adapters for objective and camera

<sup>†</sup> s.udrea@gsi.de

Content from this work may be used under the terms of the CC BY 3.0 licence (© 2018). Any distribution of this work must maintain attribution to the author(s), title of the work, publisher, and DOI.

The use of a relay lens allows for maximum flexibility in the choice of the camera to be employed in conjunction with the intensifier and also makes several image ratios possible (values of 18:8, 18:11, 25:8, 25:11 are recommended by the manufacturer).

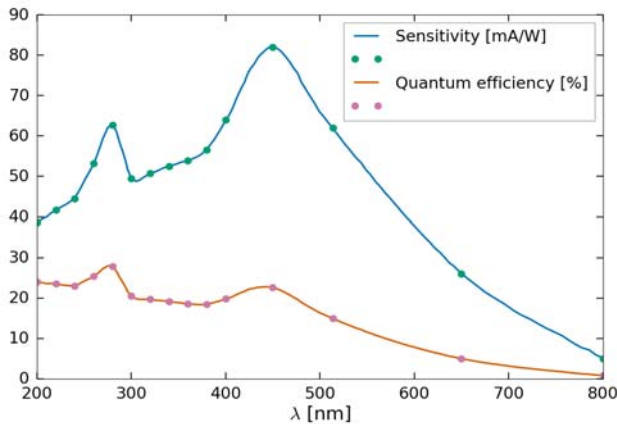


Figure 2: Wavelength dependency of sensitivity and quantum efficiency for the UV enhanced S20 photocathode according to the manufacturer.

For the prototype beam diagnostics set-up a BASLER acA1920-40gm CMOS camera has been chosen. It uses a Sony IMX249 chip with an 11.25 x 7.03 mm sensitive area and a resolution of 1920 x 1200 pixels. The minimum exposure time is 40 μs@12-bit and a maximum frame rate of 42 fps can be achieved. No upper limit is specified for the exposure time, which can be set by the duration of the trigger pulse.

### THE LENS SYSTEM

The resolution of the intensified camera system is 28 lp/mm at the phosphor screen. Due to the small transversal size of the proton and electron beams to be

measured one can still manage a proper resolution in object space if the magnification is large enough. The lens should also collect as much light as possible to keep integration times low. These conditions lead to a small depth of field (DOF) [1]. This is relevant if a typical geometry is chosen in which the gas curtain is at 45° to both the beam and optical axes. For the prototype set-up this is the envisaged geometry and thus one has to find an appropriate compromise, for which a 40 mm diameter apochromatic triplet optimised for a magnification of 1 has been acquired from Bernhard Halle Nachfl. GmbH. The focal length is 160 mm resulting in a working distance of about 320 mm at nominal magnification. To reduce geometrical errors and provide for a larger DOF an iris with a maximum opening of Ø 25 mm has been mounted in front of the lens. This leads to a maximum solid angle of  $4\pi \cdot 3.8 \cdot 10^{-4}$  sr, corresponding to only 0.038 % of the total emission sphere, at nominal magnification.

To assess the expected resolution, simulations have been performed with ZEMAX. These show that, in the case of a source emitting broad spectrum radiation from 300 to 700 nm, the lens provides a resolution of up to about 40 lp/mm. Nevertheless, since measurements will be performed with filters limiting the spectral range to that of interest, a better resolution can be achieved. Thus the lens has a relatively small effect on the overall resolution of the detection and imaging set-up which is mainly determined by that of the image intensifier.

The complete optical arrangement is presented in Fig. 3. The 60 mm cage system manufactured by THORLABS allows for accommodating the 40 mm lens and for proper alignment of the optical elements including a filter wheel. Due to the single photon detection scheme the optical path and the filter wheel are shielded from stray light by bellows and a custom housing respectively.

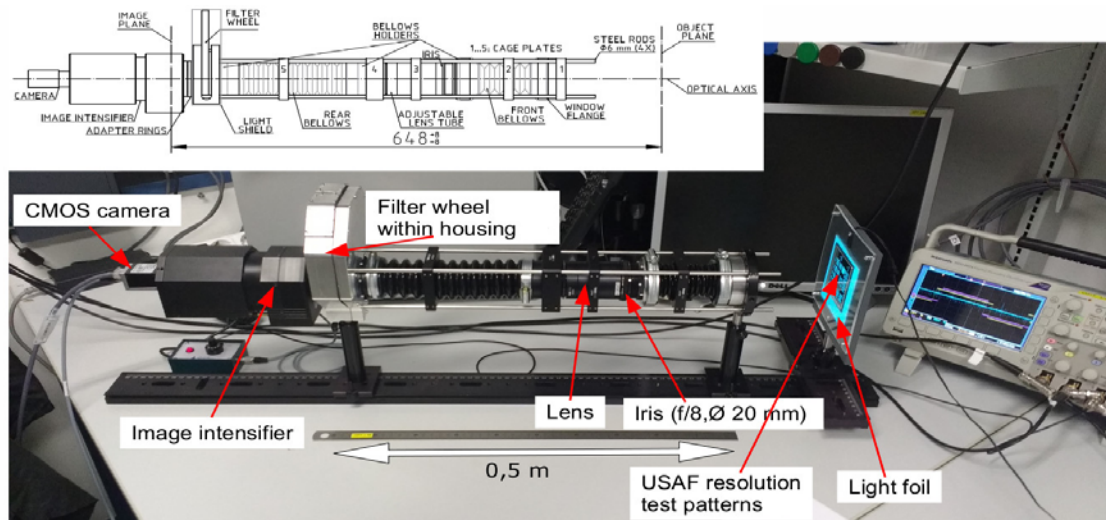


Figure 3: Complete detection and imaging set-up as used for tests at the GSI.

## COMMISSIONING

First tests of the complete detection and imaging set-up (Fig. 3) were performed at the GSI. This included: resolution measurements with and without image intensifier, depth of field measurements, assessment of the background due to dark counts and stray light. For all measurements the iris had an opening of  $\varnothing$  20 mm.

To determine the achievable resolution a USAF 1951 glass test chart has been employed, backlit by means of a light foil. This test chart consists of patterns arranged in numbered groups. Each group contains six numbered elements with each element including one horizontal and one vertical pattern of the same resolution  $R$ , which can be computed in lp/mm according to [3]:

$$R = 2^G \cdot 2^{\frac{E-1}{6}}$$

Here  $G$  and  $E$  are the group and element number respectively.

Without image intensifier the limiting resolution of the optical system has been assessed to be 57 lp/mm, which is larger than that predicted by simulation. This can be explained by the fact that the emission of the light foil has a relatively narrow spectrum and that the test set-up had a magnification of approximately 1.2. With the image intensifier used in imaging mode (lowest amplification) the best resolution one can expect is 20 lp/mm. A comparison of these two cases is shown in Fig. 4.

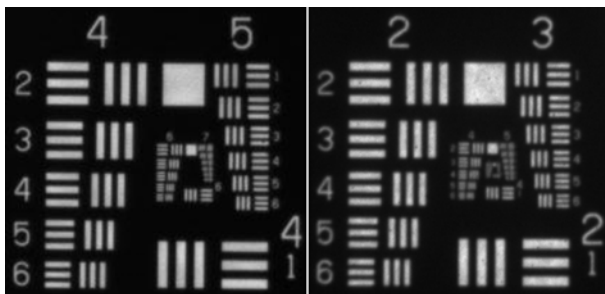


Figure 4: Images of the USAF 1951 test chart obtained without (left) and with (right) image intensifier. Resolution increases with group (top) and element number (side). Due to the difference in resolution, the two images show different groups of patterns.

For assessing the DOF the USAF 1951 test chart was displaced along the optical axis until the resolution dropped to about 10 lp/mm in the image obtained without the intensifier. This resulted in a value of  $4.5 \pm 0.5$  mm. If this should prove insufficient one may consider a set-up with the optical axis perpendicular to the gas curtain or a so called Scheimpflug configuration [4].

The background level due to dark counts and stray light was also investigated. To obtain an estimation of the number of dark counts to be expected, the image intensifier was detached from the set-up and used in photon counting mode (maximum amplification) with the input closed by its protective cap. For a gate time of 40 ms 124 counts were identified. Taking into

consideration the imaging ratio of the relay lens and the size of the CMOS detector this results in  $886 \pm 60$  counts/cm<sup>2</sup>/s. With the image intensifier attached to the set-up with its input covered, 520 counts were identified, corresponding to  $3714 \pm 120$  counts/cm<sup>2</sup>/s. Since in both cases the illumination of the laboratory was kept at usual levels, the difference between the two measurements arises from imperfections in the stray light shield of the set-up. This can be mitigated by improving the shielding or reducing the environmental light level.

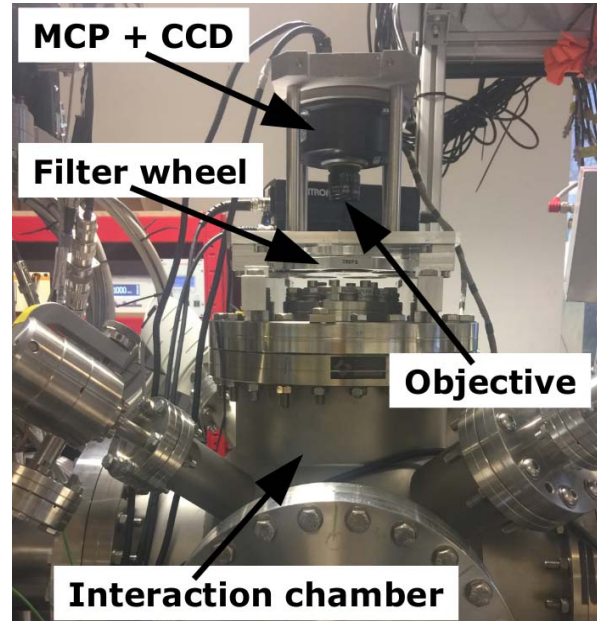


Figure 5: The set-up used for preparatory experiments during the development of the prototype for the future BIF detection and imaging installation.

## PREPARATORY EXPERIMENTS

During the development phase of the prototype a series of measurements were performed using the existing gas jet curtain installation at the Cockcroft Institute [5] with equipment already available at the GSI [6]. The BIF detection and imaging set-up was composed of a ProxiVision image intensifier with a double MCP in

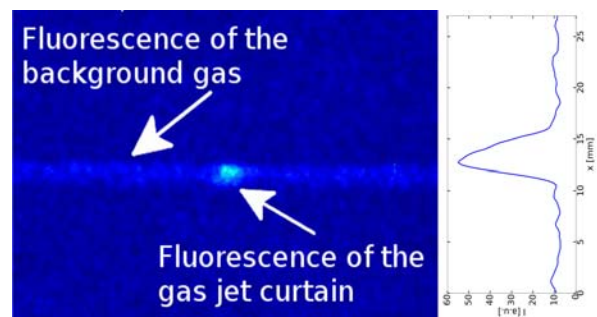


Figure 6: Profile of a 3.5 keV electron beam due to its interaction with a supersonic N<sub>2</sub> gas curtain. The profile appears enlarged due to the low spatial resolution of the optics used in the preparatory experiments.

Content from this work may be used under the terms of the CC BY 3.0 licence (© 2018). Any distribution of this work must maintain attribution to the author(s), title of the work, publisher, and DOI.

Chevron configuration coupled through fiber optics to a Basler A311f CCD camera. This was combined with a Pentax B2528-UV objective with  $f=25$  mm and  $F\#=2.8-16$ , having a transmission band from 230 to 800 nm, and a filter wheel with four 10 nm bandwidth filters at 337, 390, 430 & 470 nm, see Fig. 5. The electron gun used at the time provided only 10  $\mu$ A of beam current at a maximum energy of 5 keV. The transverse profile of this beam was estimated to have a width of about 1 mm. The density of the gas jet curtain was  $\approx 2.5 \cdot 10^{-10}$   $\text{cm}^{-3}$  [5]. Due to the low electron current and small aperture of the objective very long exposure times of up to 8000 s were needed for the successful generation of images, Fig. 6. To improve on this in future experiments, it is foreseen to increase the electron current up to 300  $\mu$ A at 10 keV.

## NEON AS WORKING GAS

Because of considerations related to the vacuum system at the HL-LHC, Neon might be a better choice than Nitrogen as working gas. We will briefly present here the estimations made for the fluorescence cross-section corresponding to the strongest emission line of neutral Ne, which is due to the  $2s^2 2p^5 ({}^2P^{\circ}_{1/2}) 3p^2 [{}^1S_0]_0 \rightarrow 3s^2 [{}^1S_0]_1$  (Paschen notation:  $2p_1 \rightarrow 1s_2$ ) transition at 585.4 nm [7]. The Ne atom is also of special interest, because its movement during the time spent in the upper excited state is not influenced by the electric and magnetic fields of the charged particle beams and the solenoid. Moreover this lifetime is  $\approx 15$  ns [8], four times shorter than that of the relevant  $\text{N}_2$  state [9].

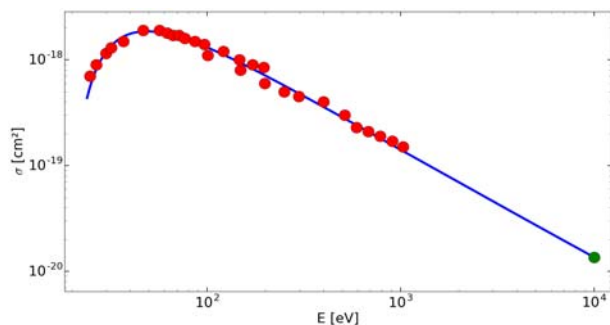


Figure 7: Fluorescence cross-section for electrons and Ne as working gas. Red dots: data from literature; fit and extrapolation: blue line and green dot.

Fluorescence cross-sections are available for Neon up to an energy of 1 keV for electrons and 1 MeV for protons [7,10]. For electrons the extrapolation to 10 keV is performed using a formula similar to the one proposed in [11]:

$$\sigma_{585}^e = \frac{8 \cdot \pi \cdot a_0^2 \cdot R}{m_e \cdot c^2} \cdot F \cdot \left[ \frac{1 - \left( D \cdot \frac{1}{\beta^2} \right)^u}{1 - D^u} \right]^v \cdot \left[ \frac{1}{\beta^2} \right]^w$$

$F$ ,  $u$ ,  $v$  and  $w$  are fit parameters,  $a_0$  the Bohr radius,  $R$  the Rydberg constant,  $m_e$  the electron rest mass,  $c$  the speed of

light in vacuum,  $\beta$  the electron's speed divided by  $c$ ,  $D = 2 \cdot W / (m_e \cdot c^2)$ , and  $W$  the excitation energy of the  $2p_1$  level with respect to the ground state. Figure 7 shows the available experimental data together with the corresponding fit and extrapolation with  $F \approx 2.5 \cdot 10^{-2}$ ,  $u \approx 1.75$ ,  $v \approx 2.49$  and  $w \approx 1.03$ . Thus the fluorescence cross-section  $\sigma_{585}^e$  has an estimated value of  $1.4 \cdot 10^{-20}$   $\text{cm}^2$ . Considering a gas curtain with a density of  $2.5 \cdot 10^{-10}$   $\text{cm}^{-3}$ , a thickness of 0.5 mm and using parameters as for the prototype set-up described above, the expected average photon detection time is  $1.1 \cdot 10^{-3}$  s/photon for a 5 A electron beam, still more than sufficient to give a good image on second timescales. In comparison, Nitrogen fluorescence at 391.4 nm would result in an average photon detection time of about  $4 \cdot 10^{-6}$  s/photon under otherwise identical conditions.

Presently, the only way to estimate the cross-section for 7 TeV protons is by the principle of equal velocities, i.e. from the cross-section for 3.8 GeV electrons. This results in  $\sigma_{585}^p \approx 4.7 \cdot 10^{-22}$   $\text{cm}^2$  by the above formula. The detection time thus estimates to 0.15 s/photon for a proton beam with an average current of 1 A, compared to  $\approx 5 \cdot 10^{-4}$  s/photon in the case of Nitrogen. Several minutes would therefore be necessary to acquire decent images of the proton beam with Ne as target gas.

## CONCLUSION

A prototype BIF detection and imaging set-up for transverse beam diagnostics on electron lenses has been developed and successfully tested offline. First preparatory experiments with  $\text{N}_2$  as working gas lead to promising results. Detection times for photons emitted by Ne at 585.4 nm have been estimated based on available cross-section data and extrapolation to higher energies and further experiments are now planned both with  $\text{N}_2$  and Ne following the installation of an upgraded electron gun.

## ACKNOWLEDGEMENT

S. Udrea and P.Forck acknowledge the support of C. Andre with the realisation of the test set-up at the GSI.

## REFERENCES

- [1] S. Udrea *et al.*, in *Proc. IBIC'16*, pp. 529-532.
- [2] Y. Shutko *et al.*, in *GSI Sci. Rep. 2014*, p. 463.
- [3] USAF 1951, [https://en.wikipedia.org/wiki/1951\\_USAF\\_resolution\\_test\\_chart](https://en.wikipedia.org/wiki/1951_USAF_resolution_test_chart)
- [4] Ch. Wiebers *et al.*, in *Proc. IBIC'13*, pp. 807-810.
- [5] V. Tzoganis and C. P. Welsch, *Appl. Phys. Lett.*, vol. 104, p. 204104, 2014.
- [6] C. Andre *et al.*, in *Proc. DIPAC'11*, pp. 185-187.
- [7] M. Eckhardt, D. Hasselkamp, and K.-H. Schartner, *Z. Physik A*, vol. 292, pp. 337-345, 1979.
- [8] A. Kramida, Yu. Ralchenko, J. Reader, and NIST ASD Team (2015), NIST Atomic Spectra Database (ver. 5.3), <http://physics.nist.gov/asd>

- [9] M. A. Plum, E. Bravin, J. Bossler, and R. Maccaferri, *Nucl. Instr. Meth. A*, vol. 492, pp. 74-90, 2002.
- [10] J.E. Chilton, M.D. Stewart, Jr., and C.C. Lin, *Phys. Rev. A*, vol. 61, pp. (052708)1-12, 2000.
- [11] V. Puech and S. Mizzi, *J. Phys. D: Appl. Phys.*, vol. 24, pp. 1974-1985, 1991.